

# Giant current-driven domain wall mobility in (Ga,Mn)As

Anh Kiet Nguyen, Hans Joakim Skadsem, and Arne Brataas

*Department of Physics, Norwegian University of Science and Technology, N-7491, Trondheim, Norway*

We study theoretically current-driven domain wall dynamics in (Ga,Mn)As. We show that the effective spin-orbit coupling of the holes qualitatively changes the domain wall dynamics and that standard spin transfer torque descriptions are inapplicable for (Ga,Mn)As. The strong effective spin-orbit coupling causes significant hole reflection from the domain wall, resulting in spin accumulation and mistracking between current-carrying spins and the domain wall magnetization. This strongly enhances the spin transfer torque and increases the current-driven domain wall mobility by four orders of magnitude, which is close to experimental findings.

Spin-polarized currents can reverse the magnetization, excite spin-waves or move domain walls in ferromagnets. These are intriguing phenomena which can become useful in digital memory and data storage. Ferromagnetic semiconductors are especially interesting because the critical current density required to move domain walls is two to three orders of magnitude smaller than in ferromagnetic metals [1, 2, 3, 4]. Great efforts have been invested both experimentally [1, 2, 3, 4, 5, 6, 7, 8, 9] and theoretically [10, 11, 12, 13, 14, 15, 16] in order to gain an understanding of current-driven domain wall dynamics [18]. However, it is not understood why the critical current density for domain wall motion is so low in ferromagnetic semiconductors compared to conventional ferromagnetic metals. We provide an answer to this important question.

In ferromagnetic metals, the domain wall width  $\lambda_w$  is large compared to the Fermi wave length  $\lambda_F$ , and the spin-orbit coupling is weak. The domain wall causes no electron reflection when  $\lambda_w \gg \lambda_F$  and the electrons adiabatically align their magnetic moments with the local magnetization direction as they propagate through the domain wall. In other words, any out-of-equilibrium spin-current density is always parallel to the magnetization direction in the domain wall,  $\mathbf{j}_s(y) = \mathbf{m}(y)j_s(y)$ , where  $\mathbf{m}$  is a unit vector along the magnetization direction of the domain wall and  $j_s \propto \hbar j/e$  is the spin-current magnitude at position  $y$  along the domain wall. Here,  $j$  and  $e$  are the charge current density and the elementary charge, respectively. When there is no spin-flip relaxation, conservation of total angular momentum dictates that the loss of spin-current along the domain wall is transferred to the magnetization order parameter as an adiabatic spin-transfer torque  $\Delta y \mathcal{T}_a = \mathbf{j}_s(y + \Delta y) - \mathbf{j}_s(y)$  [10, 12, 14, 15, 19]:

$$\mathcal{T}_a = -j_s \mathbf{m} \times [\mathbf{m} \times (\hat{\mathbf{j}} \cdot \nabla) \mathbf{m}]. \quad (1)$$

Here,  $\hat{\mathbf{j}}$  is a unit vector along the charge current direction. This adiabatic approximation, in which the spin of all charge carriers is assumed to be parallel to the magnetization of the domain wall, have been extensively used in theoretical studies of domain wall dynamics [10, 14, 15, 19]. It has been found that current densities below a critical current density  $j_c$  cannot induce

steady-state motion of the domain wall in the adiabatic limit ( $\lambda_w \gg \lambda_F$ ), even without impurity pinning [10, 19]. Steady-state domain wall motion only occurs when 1) the current density is larger than  $j_c$  and the domain wall cannot compensate the current-driven spin-torque by out-of-plane tilting [10, 15] or 2) there exists non-adiabatic terms from *e.g.* spin-flip mechanisms [11, 12] or spin-waves [13, 19]. Such non-adiabatic contributions [11, 12] can be expressed as

$$\mathcal{T}_{na} = -\beta j_s \mathbf{m} \times (\hat{\mathbf{j}} \cdot \nabla) \mathbf{m}, \quad (2)$$

where  $\beta$  is a small, dimensionless parameter that describes non-adiabaticity.

In this Letter, we will show that the strong (Ga,Mn)As *effective spin-orbit interaction introduces a new, intrinsic, non-adiabatic spin transfer torque that completely dominates the domain wall dynamics*. The non-adiabatic mechanism to be discussed cannot be described by Eqs.(1) and (2). Furthermore, we find that the steady-state domain wall drift velocity  $v_w$  is proportional to the current density, at small current densities. The interesting quantity is the current-driven domain wall mobility

$$\mu_I = v_w/j. \quad (3)$$

For realistic values of domain wall width and spin-orbit coupling strength, we find that  $\mu_I$  is enhanced by four orders of magnitude compared to a system without, or with only weak spin-orbit interaction, *e.g.* conventional ferromagnets. This may explain an important phenomena under discussion, namely why  $j_c$  ( $\mu_I$ ) is so much smaller (larger) in (Ga,Mn)As as compared to conventional ferromagnetic metals [1, 2, 3, 4].

The origin of the giant current-driven domain wall mobility is the spin-orbit interaction. Radically different than in conventional ferromagnets, the strong intrinsic (Ga,Mn)As spin-orbit interaction causes a finite domain wall resistance even in the adiabatic limit, by preventing a large fraction of carriers to adiabatically adjust their spins to the magnetization of the domain wall [20, 21]. This effect is similar to the anomalous magnetoresistance in ferromagnets. The intrinsic domain wall resistance induces spin accumulation and mistracking between carrier

spins and the magnetization of the domain wall, rendering the approximations Eqs.(1) and (2) inapplicable, at least in the ballistic limit.

Our qualitative new findings do not rely on the specific microscopic model of ferromagnetic zincblende semiconductors. In order to be specific, we use the simplest model we believe captures the essential strong spin-orbit interaction, the 4-band Kohn-Luttinger Hamiltonian in the spherical approximation [20, 22, 23, 24]:

$$H = \frac{\hbar^2}{2m} \left[ \left( \gamma_1 + \frac{5}{2} \gamma_2 \right) p^2 - 2\gamma_2 (\mathbf{p} \cdot \mathbf{S})^2 \right] - \mathbf{h}(\mathbf{r}) \cdot \mathbf{S}, \quad (4)$$

where,  $m$  and  $\mathbf{p}$  are the bare electron mass and the hole momentum operator, respectively. Furthermore,  $\mathbf{S}$  is a vector of  $4 \times 4$  dimensionless angular momentum operators for a  $S=3/2$  spin, and  $\gamma_1$  and  $\gamma_2$  are Luttinger parameters. In Eq.(4),  $\mathbf{h}$  represents the exchange field from the localized magnetic moments. Eq.(4) and its 6-band version explains many features of zincblende magnetic semiconductors [25, 26, 27, 28, 29]. In our effective hole model, the parameter  $\gamma_2$  determines the strength of the effective spin-orbit coupling of the holes, which should not be mistaken for the bare electron spin-orbit coupling of relativistic origin. In order to identify effects of the spin-orbit interaction, it is useful to consider the limit  $\gamma_2=0$ , which strongly resembles the parabolic free electron models without spin-orbit interaction.

Typical length, velocity, and energy for Eq.(4) are the Fermi wave length divided by  $2\pi$  ( $\lambda_{F0}/2\pi$ ), the Fermi velocity ( $v_{F0}$ ) and Fermi energy ( $\epsilon_{F0}$ ) for heavy holes in GaAs for a given doping.

To model the dynamics of domain walls we use the following dimensionless phenomenological Landau-Lifshitz-Gilbert (LLG) equation

$$\frac{d\mathbf{m}}{d\tilde{t}} = -\mathbf{m} \times \tilde{\mathbf{h}}^{eff} + \alpha \mathbf{m} \times \frac{d\mathbf{m}}{d\tilde{t}}. \quad (5)$$

Here,  $\mathbf{m}(y) = \mathbf{h}(y)/h_0$  should be understood as a unit macrospin for the transverse slice located at  $y$ , and  $\alpha$  is the Gilbert damping constant. The dimensionless time is  $\tilde{t}=t/t_0$  where  $t_0=M_s(\lambda_{F0}/2\pi)^2/2\gamma A$ . Here,  $M_s$ ,  $A$  and  $\gamma=e/m$  are the saturation magnetization, spin stiffness and the gyromagnetic ratio, respectively. The effective dimensionless magnetic field is

$$\tilde{\mathbf{h}}^{eff} = \tilde{\nabla}^2 \mathbf{m} + \tilde{\mathbf{h}}^{an} \cdot \mathbf{m} - h_{pd} \chi_S, \quad (6)$$

where  $\tilde{\nabla} = (\lambda_{F0}/2\pi)\nabla$  and  $\tilde{\mathbf{h}}^{an}$  is the dimensionless anisotropy field, which is used to control the type and the width of the domain-wall. Demagnetization fields for simple geometries may be included in  $\tilde{\mathbf{h}}^{an}$ . Note that the energy scale for the spin stiffness is absorbed into  $\tilde{t}$ . The last term in Eq.(6) is the effective magnetic field due to the out-of-equilibrium itinerant holes which gives rise to the spin-transfer torque in the LLG equation (5)[13, 17].

The dimensionless coupling constant  $h_{pd}$  and the spin-density response function  $\chi_S$  are defined below. The LLG equation is numerically integrated from  $\tilde{t}$  to  $\tilde{t} + \Delta\tilde{t}$  using a fourth-order Runge-Kutta scheme [31].

To study transport properties, we consider the *linear response* around the Fermi energy ( $\epsilon_F$ ), measured from the bottom of the lowest band, at low temperature. Our system is a discrete, rectangular conductor of lengths  $L_x$ ,  $L_y$ ,  $L_z$  and lattice constants  $a_x$ ,  $a_y$ ,  $a_z$ , sandwiched between two reservoirs. Born-von Karman boundary conditions are applied for the transverse directions  $x$  and  $z$ . The exchange field is assumed to have a constant amplitude,  $|\mathbf{h}(\mathbf{r})|=h_0$ , and to be homogeneous in the transverse direction, *i.e.*  $\mathbf{h}(\mathbf{r})=\mathbf{h}(y)$ . We calculate the conductance using Eq.(4), the standard Landauer-Büttiker formula and a stable transfer matrix formalism [20, 30]. The transfer matrix method also provides us with the current carrying wavefunction, which is used to calculate the spin density response function. There are equilibrium and out-of-equilibrium spin densities,  $\langle \rho \mathbf{S} \rangle = \langle \rho \mathbf{S} \rangle^{eq} + \langle \rho \mathbf{S} \rangle^{ne}$ , where  $\rho$  is the density operator. The equilibrium spin density  $\langle \rho \mathbf{S} \rangle^{eq}$  is parallel to  $\mathbf{m}$  and does not contribute to the spin-transfer torque. The non-equilibrium spin density  $\langle \rho \mathbf{S} \rangle^{ne}$  is proportional to the current density and is determined as a trace over all hole states between  $\epsilon_F$  and  $\epsilon_F + eV$  in the left reservoir. The linear response function for the spin density may then be defined as  $\chi_S = (ev_{F0}/j)\langle \rho \mathbf{S} \rangle^{ne}$ , which dictates  $h_{pd} = \hbar h_0 \lambda_{F0} j / 8\pi e A \epsilon_{F0}$ , that is proportional to the current density. We use  $h_{pd}$  to control the current density [13]. Similarly, we also compute the out-of-equilibrium spin current  $\mathbf{j}_s$  and the average spin per conducting holes,  $\langle \mathbf{S}(y) \rangle = \mathbf{j}_s e / j \hbar$ .

The parameters describing our discrete conductor are  $a_x/(\lambda_{F0}/2\pi) = a_z/(\lambda_{F0}/2\pi) = 0.2$ ,  $a_y/(\lambda_{F0}/2\pi) = 0.75$ ,  $L_x=L_z=51a_x$  and  $L_y=400a_y$ . Furthermore,  $h_0/\epsilon_{F0}=1.5$ ,  $\epsilon_F/\epsilon_{F0}=2.25$ ,  $\tilde{h}_x^{an}=0$ ,  $\tilde{h}_y^{an}=-1$ . We use  $\tilde{h}_z^{an}$  to control the width of the domain wall,  $\lambda_w/(\lambda_{F0}/2\pi)=\sqrt{1/\tilde{h}_z^{an}}$ . We set the anisotropy/demagnetization field  $\tilde{h}_y^{an}=-1$ , similar to Ref.[13], for simplicity and to ensure that the considered domain walls are Bloch walls, consistent with recent experiments [1, 2, 5]. The Gilbert damping constant is set to  $\alpha=0.03$ , a midrange value for (Ga,Mn)As [32].

The calculation proceeds as follows: First, we find the zero-current stationary equilibrium configuration of the domain wall by integrating Eq.(5) with  $h_{pd}=0$  to a sufficiently large time. The equilibrium domain wall configuration is given by  $m_x(y)=1/\cosh(y/\lambda_w)$ ,  $m_y(y)=0$  and  $m_z(y)=\tanh(y/\lambda_w)$ , as expected from an analytical fixed point solution of Eq.(5). Second, a constant current is applied through a finite  $h_{pd}$ , and the following two steps are iterated: 1) compute  $\chi_S$  for a given  $\mathbf{h}=h_0\mathbf{m}$  using Eq.(4), and 2) integrate  $\mathbf{m}=\mathbf{h}/h_0$  at time  $\Delta\tilde{t}$  using Eq.(5). We use  $\Delta\tilde{t}=0.2$ , which is sufficient for convergence.

In our approach, the transfers of momentum and an-

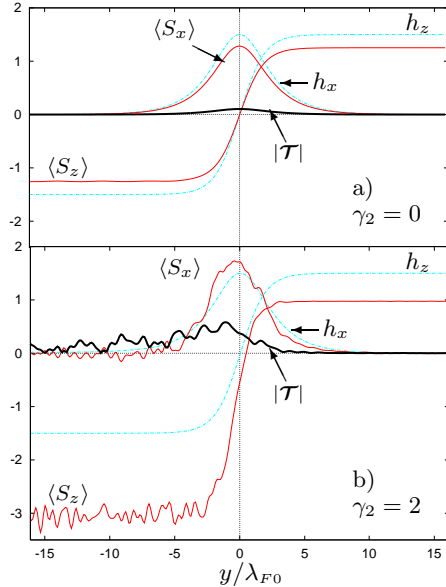


FIG. 1: Snapshots of the exchange field of the domain wall ( $h_x/\epsilon_{F0}$  and  $h_z/\epsilon_{F0}$ ), spin per conducting hole ( $\langle S_x \rangle$  and  $\langle S_z \rangle$ ) and spin-torque amplitude per conducting hole  $|\mathcal{T}|$  as functions of position, for a) zero hole spin-orbit coupling, and b) finite hole spin-orbit coupling. Snapshots are taken in steady-state. For both plots,  $h_{pd}=0.001$  and  $\lambda_w/\lambda_{F0}=2$ .

angular momentum from the carriers to the domain wall are treated on an equal footing. For all parameters considered, the domain wall is found to move in the opposite direction of the current, consistent with experimental findings [1, 2, 3].

Let us first consider a system without spin-orbit interaction. We consider a domain wall width  $\lambda_w/\lambda_{F0}=2$ , which is close to the adiabatic limit. Numerical calculation of the conductance show that only 0.1% of the incoming holes are reflected back by the domain wall. From Fig.1a, we see that the hole spins follow the domain wall magnetization closely, and  $\langle \mathbf{S}(y) \rangle$  is virtually parallel to  $\mathbf{h}(y)$  throughout the system. Outside the wall,  $\langle S_z \rangle \approx \pm 1.25$ , since both the heavy ( $S_z=1.5$ ) and light ( $S_z=0.5$ ) holes participate in the transport. The amplitude of the dimensionless spin-torque per conducting holes  $\mathcal{T}=(\mathbf{h}/\epsilon_{F0}) \times \chi_S$  is shown in Fig.1a. It fits nicely to the adiabatic spin transfer torque expression Eq.(1) through the relation  $\mathcal{T}=\mathcal{T}_a e \lambda_{F0} / 2\pi j \hbar$ .

As shown in Fig.1b, turning on the spin-orbit interaction completely changes the physical picture. Numerical calculation of the conductance shows that the intrinsic domain wall resistance forces 45% of the incoming holes to reflect, causing spin accumulation and mistracking of carrier spins and the magnetization of the domain wall, particularly in front of the wall. Interference between incoming and reflected holes creates a spin-wave pattern in  $\langle \mathbf{S} \rangle$  and  $\mathcal{T}$ . The shape of the domain wall is, however, virtually unchanged, due to the small current applied,

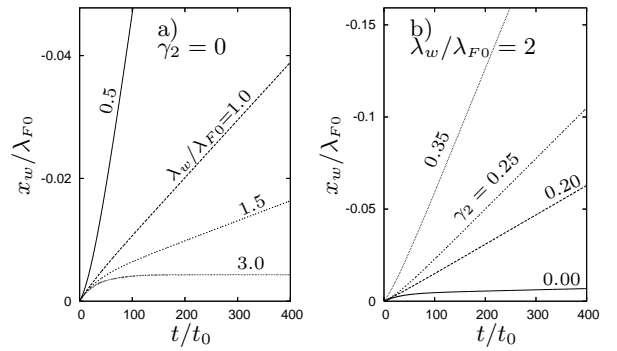


FIG. 2: Domain wall displacement as a function of time for a) zero spin-orbit coupling for varying domain wall widths, and b) fixed domain wall width for varying hole spin-orbit coupling strengths. For both plots,  $h_{pd} = 0.001$ .

$h_{pd}=0.001$ . From our previous study, we know that the majority of reflected holes consists of heavy holes [20], in agreement with  $\langle S_z \rangle \approx -3.0$  on the left side of the domain wall. The reflection causes spin accumulation and mistracking and, thereby, enlarges the amplitude of the torque with a factor of 5 compared to an identical system without spin-orbit interaction. From the large mismatch between carrier spins and the magnetization of the domain wall, one may thus conclude that spin-orbit coupling renders the standard adiabatic approximation [11, 12, 14, 19], leading to Eqs.(1) and (2) inapplicable, at least in the ballistic limit.

Fig.2a shows the domain wall displacement as a function of time for varying domain wall widths for the case of no spin-orbit interaction. The domain wall displacement completely saturates in the adiabatic limit,  $\lambda_w/\lambda_{F0} > 3$ , as expected [10, 13, 19]. Away from the adiabatic limit, *i.e.* reducing the domain wall width, an increasing fraction of holes will reflect causing spin accumulation and mistracking between the spins and the magnetization of the domain wall. This introduces a non-adiabatic torque on the domain wall and gives it a finite drift velocity, which, as can be seen in Fig.2a, increases for decreasing domain wall width.

Let us now consider a finite spin-orbit coupling. Fig.2b shows the domain wall displacement as a function of time for varying spin-orbit couplings. We see that a larger spin-orbit coupling also increases the domain wall drift velocity due to the increased reflection of holes. The reflected holes increase the spin accumulation and mistracking. This in turn increases the spin-torque on the domain wall and increases its drift velocity.

Fig.3a shows the domain wall drift velocity as a function of  $h_{pd}$  for varying spin-orbit coupling strength. We see that  $v_w$  is proportional to  $h_{pd}$  (*i.e.* the current density). Experimentally, the domain wall drift velocity also seems to increase linearly with current [1] consistent with our results, and in contrast to  $v_w \propto \sqrt{j^2 - j_c^2}$  found using

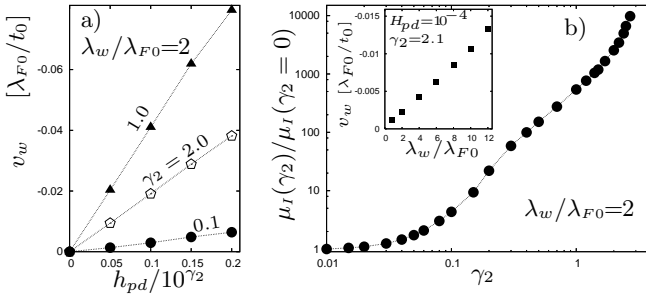


FIG. 3: a) Domain wall drift velocity as a function of  $h_{pd}$  for varying spin-orbit couplings,  $\gamma_2$ . Note that the scale of the horizontal axis is different for each spin-orbit coupling, done to collect all graphs into a single plot. b) Current-driven domain wall mobility as a function of spin-orbit coupling. Inset b) Domain wall drift velocity a function of domain wall width. For all plots, solid lines are guides for the eye.

the adiabatic approximation [10, 19]. In Fig.3b, we show the current-driven domain wall mobility as a function of spin-orbit coupling. Note that  $\mu_I(\gamma_2=0)$  for  $\lambda_w/\lambda_{F0}=2$  is small but still finite since the domain wall still reflects 0.1% of the holes giving a small non-adiabatic torque. We see that the domain wall mobility increases four orders of magnitude when the hole spin-orbit coupling increases from  $\gamma_2=0$  to an experimentally attainable value of 2.5. The domain wall width used here,  $\lambda_w/\lambda_{F0}=2$  is close to the experimental values [1, 2].

Another feature which clearly shows that strong spin-orbit coupling induces a spin-transfer torque which is completely different from the adiabatic Eq.(1) and the lowest order non-adiabatic Eq.(2) expressions is shown in the inset of Fig.3b. Here, we show the domain wall drift velocity as a function of the domain wall width for a system with spin-orbit coupling. We see that  $v_w$  increases for increasing  $\lambda_w$ , in contrast to Eq.(2) which provides a constant drift velocity [11, 12]. The region where the mistracking between the spins and the domain wall gives a net torque increases linearly with  $\lambda_w$ , while the intrinsic domain wall resistance is independent of  $\lambda_w$ . Thus,  $v_w$  should increase linearly with respect to  $\lambda_w$ .

We have not included effects of impurities [33]. However, there is an intrinsic domain wall resistance even in the diffusive transport regime, although with a reduced amplitude [34]. Thus, we expect that the spin-orbit induced effects presented in this paper also play an important role for current-driven domain wall dynamics in the diffusive transport regime when the mean free path is not much smaller than  $\lambda_w$ . Impurities are expected to introduce a critical current density and significantly reduce the domain wall drift velocity. This expected impurity induced reduction of the domain wall drift velocity is consistent with recent experimental findings [1, 2, 3]. Experiments find a two to three orders of magnitude enhancement of the drift velocity, which is smaller than our computed four order of magnitude enhancement in

the ballistic regime. Furthermore, a finite mean free path will limit the seemingly unbounded growth of  $v_w$  for increasing  $\lambda_w$  as shown in the inset of Fig.3b.

In summary, we have shown that intrinsic spin-orbit coupling completely changes the current-driven domain wall dynamics. The effective spin-orbit interaction of the holes increases the fraction of reflected carrier spins, causing spin accumulation and mistracking between carrier spins and the magnetization of the domain wall. This effect enhances the current-driven spin-torque on the domain wall. The domain wall drift velocity is found to be proportional to the current density. The domain wall current-mobility increases four orders of magnitude when the spin-orbit coupling increases from  $\gamma_2=0$  to an experimentally attainable value of 2.5.

We thank Y. Tserkovnyak, G. E. W. Bauer, and J. Hove for stimulating discussions and K. Olaussen for use of the Linux cluster. This work has been supported by the Research Council of Norway through grants no. 167498/V30, 162742/V00, 1585181/143, and 1585471/431.

---

- [1] M. Yamanouchi *et al.*, Phys. Rev. Lett. **96**, 96601 (2006).
- [2] M. Yamanouchi *et al.*, Nature **428**, 539 (2004).
- [3] C. Gould *et al.*, cond-mat/0602135 (2006).
- [4] A. Yamaguchi *et al.*, Phys. Rev. Lett. **92**, 077205 (2004).
- [5] D. Chiba *et al.*, Phys. Rev. Lett. **96**, 096602 (2006).
- [6] P. P. Freitas and L. Berger, J. App. Phys. **57**, 1266 (1985).
- [7] L. Gan *et al.*, IEEE Trans. Magn. **36**, 3047 (2000).
- [8] J. Grollier *et al.*, App. Phys. Lett. **83**, 509 (2003).
- [9] E. Saitoh *et al.*, Nature **432**, 203 (2004).
- [10] G. Tatara and H. Kohno, Phys. Rev. Lett. **92**, 086601 (2004).
- [11] S. Zhang and Z. Li, Phys. Rev. Lett. **93**, 127204 (2004).
- [12] A. Thiaville *et al.*, Europhys. Lett. **69**, 990 (2005); Y. Tserkovnyak, A. Brataas, and G. E. W. Bauer, cond-mat/0512715; H. Kohno, G. Tatara and J. Shibata, cond-mat/0605186.
- [13] J. Ohe and B. Kramer, Phys. Rev. Lett. **96**, 27204 (2006).
- [14] Y. B. Bazaliy, B. A. Jones, and S.-C. Zhang, Phys. Rev. B **57**, R3213 (1998).
- [15] L. Berger, Phys. Rev. B **33**, 1572 (1986).
- [16] J. C. Slonczewski, J. Magn. Magn. Mat. **159**, L1 (1996).
- [17] A. S. Núñez and A. H. MacDonald, cond-mat/0403710.
- [18] C. H. Marrows, Adv. Phys. **54**, 585 (2005).
- [19] Z. Li and S. Zhang, Phys. Rev. Lett. **92**, 207203 (2004).
- [20] A. K. Nguyen, R. V. Shchelushkin and A. Brataas, cond-mat/0601436.
- [21] R. Oszwaldowski, J. A. Majewski and T. Dietl, cond-mat/0605230.
- [22] J. M. Luttinger, Phys. Rev. **102**, 1030 (1956).
- [23] A. Baldereschi and N. O. Lipari, Phys. Rev. B **8**, 2697 (1973).
- [24] J. Schliemann, cond-mat/0604585.
- [25] T. Dietl, H. Ohno, and F. Matsukura, Phys. Rev. B **63**, 195205 (2001).

- [26] T. Dietl *et al.*, Science **287**, 1019 (2000).
- [27] M. Abolfath *et al.*, Phys. Rev. B **63**, 054418 (2001).
- [28] J. König *et al.*, in *Electronic Structure and Magnetism of Complex Materials*, edited by D. J. Singh and D. D. Papaconstantopoulos (Springer Verlag, 2002).
- [29] T. Jungwirth *et al.*, Rev. Mod. Phys. **xx**, yyyy (2006).
- [30] T. Usuki *et al.*, Phys. Rev. B **52**, 8244 (1995).
- [31] J. Z. Sun, Phys. Rev. B **62**, 570 (2000).
- [32] J. Sinova *et al.*, Phys. Rev. B **69**, 085209 (2004).
- [33] C. Timm, J. Phys.: Condens. Matter **15**, R1865 (2003).
- [34] R. V. Shchelushkin, A. K. Nguyen and A. Brataas, in preparation.